Biophysical Regulation of Lipid Biosynthesis in the Plasma Membrane

Stephen H. Alley,* Oscar Ces,† Richard H. Templer,† and Mauricio Barahona*‡
*Department of Bioengineering, †Department of Chemistry and ‡Institute for Mathematical Sciences, Imperial College London, South Kensington Campus, London, United Kingdom

ABSTRACT We present a cellular model of lipid biosynthesis in the plasma membrane that couples biochemical and biophysical features of the enzymatic network of the cell-wall-less Mycoplasma *Acholeplasma laidlawii*. In particular, we formulate how the stored elastic energy of the lipid bilayer can modify the activity of curvature-sensitive enzymes through the binding of amphipathic α-helices. As the binding depends on lipid composition, this results in a biophysical feedback mechanism for the regulation of the stored elastic energy. The model shows that the presence of feedback increases the robustness of the steady state of the system, in the sense that biologically inviable nonbilayer states are less likely. We also show that the biophysical and biochemical features of the network have implications as to which enzymes are most efficient at implementing the regulation. The network imposes restrictions on the steady-state balance between bilayer and nonbilayer lipids and on the concentrations of particular lipids. Finally, we consider the influence of the length of the amphipathic α-helix on the efficacy of the feedback and propose experimental measurements and extensions of the modeling framework.

INTRODUCTION

The primary function of the lipids in the plasma membrane is to form a bilayer that provides a permeability barrier between the cytoplasm and the environment. However, whereas lipids were once considered purely passive components, it is now clear that lipids play an active role in a variety of dynamic processes involving the membranes that compartmentalize the cell (1). To achieve this dual role of the membrane as a dynamic boundary and a continuous barrier, the cell must regulate the mechanical properties of the membrane and does so partly by controlling its lipid composition.

Membrane lipids are chemically diverse (2) but they can be classified into the broad categories of bilayer and nonbilayer lipids, depending on their (in)ability to self-assemble into bilayers. Bilayer formation is the result of a thermodynamic equilibrium in which the physicochemical properties of the lipids, such as the chemical structure of the headgroup and hydrocarbon chains, play a crucial role. The cell can therefore regulate the mechanical properties of the bilayer by modifying its lipid composition through lipid biosynthesis. The balance between bilayer and nonbilayer lipids in the plasma membrane has been the subject of many reviews (2–4). Experiments have shown that organisms change the lipid composition of their membranes in response to external variations in diet, pressure, and temperature (5–7; see also (18)). Moreover, many of the lipids found in biological membranes do not form bilayers under physiological conditions. Subsequent studies have confirmed that most organisms contain significant amounts of at least one nonbilayer lipid (8,9).

The underlying biophysical question is the relationship between the chemical diversity and variability of membrane lipid composition, the mechanical properties of the membrane, and the associated protein functions (10,11). A large experimental effort has been devoted to mapping lipid biosynthetic pathways by characterizing and mutating particular enzymes. There is also an increasing body of experiments that measure the relationship between the biophysical properties of lipids and enzyme activity (10,12). However, there have been few attempts (13) to consider theoretically the interdependence of these two phenomena by modeling the lipid biosynthetic network as an integrated system in which the biochemical and the biophysical descriptions of the metabolic network are fundamentally linked. The focus of the model presented here is to provide a set of tools to understand the interplay between the enzymes and lipids involved in lipid metabolism in relation to the biophysical properties of the bilayer.

Fig. 1 depicts a simplified representation of the connection between the chemical structure of lipids and the mechanical properties of a lipid monolayer. A lipid monolayer consists of conformationally flexible lipids, whose amphiphilic nature leads to a nonuniform pressure distribution across the monolayer. The lateral pressure profile $\pi(z)$ determines the average ''molecular shape'' that a lipid adopts and, more importantly, J_s, the monolayer spontaneous curvature. J_s is an intrinsic property of a lipid species that corresponds to the monolayer curvature in which a lipid in the monolayer is at the conformation with minimum free energy (14). The spontaneous curvature reflects the desire of a lipid monolayer to either curve away from, or curve toward, the membrane-water interface and whether a lipid is a bilayer or nonbilayer lipid.

A lipid bilayer is formed by two monolayers back-to-back. This arrangement means that the monolayers may not be able

Submitted July 27, 2007, and accepted for publication October 11, 2007.

Address reprint requests to M. Barahona, E-mail: m.barahona@imperial.ac.uk.

Editor: Thomas J. McIntosh.

0006-3495/08/04/2938/17 $2.00

doi: 10.1529/biophysj.107.118380

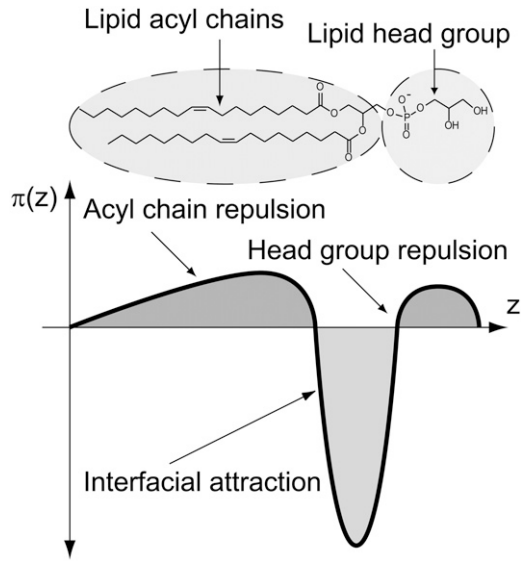

FIGURE 1 Forces that act between lipids at different depths include electrostatic and hydrogen bond interactions at the headgroup, interfacial tension at the hydrophilic-hydrophobic interface, and the packing of the hydrocarbon chains. The lateral pressure profile $\pi(z)$ depends crucially on the chemical nature of the lipid head group and the length and saturation of the lipid hydrocarbon chains. The lateral pressure profile determines the spontaneous curvature J_s of a lipid monolayer (14).

to adopt their preferred curvature, J_s, since the monolayers in the bilayer are held together by the hydrophobic effect. This leads to a difference between the actual curvature of a monolayer, as given by the principal curvatures c_1 and c_2, and its spontaneous curvature, J_s (15). Based on this physical picture, Helfrich (16) formulated the stored elastic energy per unit area, g, of a lipid monolayer that is constrained to have principal curvatures c_1 and c_2:

$$g = \frac{F}{A} = \frac{\kappa_M}{2}(c_1 + c_2 - J_s)^2,$$

where F is the Helmholtz free energy, A is the area, and κ_M is the bending rigidity of the monolayer. The lipids are at the free energy minimum, when the total curvature, $c_1 + c_2$, is at the value of the spontaneous curvature J_s. Because at equilibrium g is minimized, this means it is more difficult for lipids with large spontaneous curvatures to form a bilayer, which is a flat conformation with small c_1 and c_2. Indeed, it has been suggested that lipids with $J_s < -1/6$ nm^{-1} (the negative sign is a convention to denote that the monolayer curves toward water in an interface) do not form bilayers. Instead, they form curved mesophases, such as the inverse hexagonal phase, which are porous (17).

From a biological perspective, porous mesophases would have severe consequences for cellular function and survival. Gruner (3) hypothesized that the average spontaneous curvature J_s^{mix} of the lipids in the plasma membrane must be tightly regulated to ensure that the membrane lipids form a (nonporous) bilayer and that the cell is able to control J_s^{mix} (15) by modifying its lipid composition through the biochemical networks of lipid metabolism.

This insight has been confirmed experimentally. Lipid extracts from the cell-wall-less Mycoplasma *Acholeplasma laidlawii* grown under different conditions have average spontaneous curvatures J_s^{mix} in the small range between $-1/6.6$ nm^{-1} and $-1/8.1$ nm^{-1} even though the membrane contains lipids with J_s outside of this range (18). To achieve this robust regulation, *A. laidlawii* alters the ratio of its two main glucolipids in response to the length and saturation of exogenously fed fatty acids (5), thus maintaining J_s^{mix} in a biologically viable ''bilayer range'' that ensures membrane integrity yet with enough stored elastic energy to allow for its dynamical behavior. Remarkably, although the average spontaneous curvature is controlled, the lipid concentrations exhibit wide variations. This suggests that the control of J_s^{mix} is not achieved by targeting specific lipid compositions. These observations also apply to *Escherichia coli* lipid extracts, which begin to form nonbilayer structures close to physiological conditions (7).

Biophysical control mechanisms integrated into lipid biosynthetic networks have been the subject of intense experimental study. An example is given by cytidine triphosphate/phosphocholine cytidyltransferase (CCT), an enzyme involved in the biosynthesis of the ubiquitous lipid phosphatidylcholine. CCT is inactive in the cytoplasm, but becomes active when membrane-bound. It has been shown that its activity is affected by the stored elastic energy in the membrane (12). The biophysical control mechanism arises from the presence of an amphipathic α-helix that affects enzyme activity by regulating the binding of CCT to lipid bilayers. In a broad sense, the amphipathic α-helix can be viewed as a ''sensor'' of the spontaneous curvature since it binds preferentially to lipid bilayers with large negative J_s^{mix}, thus modulating the activity of the lipid biosynthetic enzyme. This biophysical control mechanism is chemically nonspecific, as it is based on a biophysical interaction between the enzyme and the membrane, and appears to be generic to a number of enzymes present in lipid biosynthetic pathways (12,19), including those present in *A. laidlawii*, which is the focus of this study.

We have developed a modeling framework for the lipid biosynthetic pathways in *A. laidlawii*. Building upon the *A. laidlawii* biochemical network studied in detail by the groups of Lindblom, Rilfors, and Wieslander (5,6,19,20), we formulate a biophysical mechanism, based upon some of the conceptual foundations established in CCT (12), that couples the activity of lipid biosynthetic enzymes to the membrane composition. Our results show that the presence of feedback increases the robustness of the steady state of the system to parameter variations, in the sense that it decreases the probability of inviable values of J_s^{mix} that would lead to porous phases. From a sensitivity analysis, we identify the enzymes that are most efficient in implementing the control of the network. We also study the restrictions that the network imposes on the steady-state concentrations of particular lipids

and show that the system keeps a balance between bilayer and nonbilayer lipids. Finally, we consider the influence of the length of the amphipathic α-helix on the efficacy of the feedback.

THE LIPID BIOSYNTHETIC NETWORK OF *A. LAIDLAWII*

We take the cell-wall-less Mycoplasma *A. laidlawii* as our system for the study of cellular models of lipid biosynthesis. This simple organism, which has been studied in great detail (5,6), has two features that make it ideal to showcase our modeling framework. First, virtually all the lipids in *A. laidlawii* are in the plasma membrane (21). This simplifies the model to a single lipid bilayer, avoiding the complexity of cell walls and intracellular compartments. Second, *A. laidlawii* cannot synthesize unsaturated fatty acids and is very limited in its synthesis of saturated fatty acids (5). Therefore, *A. laidlawii* exhibits a significantly reduced number of chemical species in the plasma membrane as it relies on exogenously fed fatty acids for lipid biosynthesis.

The limited fatty acid synthesis implies that the only response of *A. laidlawii* to variations in its fatty acid diet is to alter the composition of the headgroups of the lipids in the membrane through the network of enzymatic reactions represented in Fig. 2. Indeed, experiments show that the membrane lipid composition of *A. laidlawii* depends strongly on the length and saturation of exogenously fed fatty acids (5). When *A. laidlawii* is fed palmitic acid (a short, saturated fatty acid), monoglucosyldiacylglycerol (MGlcDAG) is the most abundant lipid; whereas when *A. laidlawii* is fed oleic acid (a long, unsaturated fatty acid), diglucosyldiacylglycerol (DGlcDAG) dominates. Central to our study is the observation that although the variation in the lipid composition can be large, the cell maintains the average monolayer spontaneous curvature of the plasma membrane J_s^{mix} within a ''window'' in which the bilayer phase is stable (7) (Table 1). The lipid biosynthetic network is able to adjust the lipid composition to achieve a $J_s^{mix} > -1/6\ nm^{-1}$, thus maintaining a dynamic, yet impermeable plasma membrane.

The lipid biosynthetic network: biochemical and biophysical descriptions

The biochemical description of the lipid biosynthetic network of *A. laidlawii* is presented in Fig. 2 *A*. The first step in the metabolic network is, as in other organisms, the acylation of soluble glycerol-3-phosphate (G3P) to form phosphatidic acid (PA) (22). The network then branches out into two pathways.

The upper branch is the phosphatidylglycerol (PG) pathway, well-studied in bacteria, in which PA is converted into PG through the intermediates cytidine diphosphate diacylglycerol (CDP-DAG) and phosphatidylglycerolphosphate (PGP). The corresponding enzymes CDP-DAG synthase (CDS), PGP synthase (PGPS), and PGP phosphatase (PGPP) have been characterized in *E. coli* (23,24) and in *Clostridium perfringens* (25,26).

The lower branch is a specific pathway in *A. laidlawii*, deduced from the discovery and purification of the PA phosphatase (PAP) (27) and the two consecutive glucosyltransferases, MGlcDAG synthase (MGS) (28) and DGlcDAG synthase (DGS) (29). The final enzymatic reaction is yet to be characterized since the glycerophosphoryl-DGlcDAG (GPDGlcDAG) synthase (GPDGS) that catalyzes the production of GPDGlcDAG has not been purified yet. However, the genetic similarity of MGS and DGS to the enzymes of Gram-positive bacteria (30) suggests that GPDGlcDAG could be synthesized by the transfer of G3P from PG to DGlcDAG, a reaction that occurs in the synthesis of lipoteichoic acids in the cell walls of Gram-positive bacteria (31).

Fig. 2 *B* presents a biophysical interpretation of the network, showing how the molecular shape of each lipid is reflected in its monolayer spontaneous curvature. This physical picture shows that the position of nonbilayer lipids ($J_s < -1/6\ nm^{-1}$) and bilayer lipids ($J_s > -1/6\ nm^{-1}$) within the network has an effect on which enzymes can exercise effective control of the J_s^{mix} of the plasma membrane. By inspection, MGS and DGS are good candidates for the control of J_s^{mix}, since MGS and DGS catalyze the reactions that lead from the lipid with the most negative J_s (DAG) to the lipid with the least negative J_s (DGlcDAG) (Fig. 2 *B*). This intuition is reinforced by a structural feature of these enzymes. MGS and DGS are both peripheral membrane proteins that translocate between the cytoplasm and the membrane. It is postulated that they are only active when they are inserted into the membrane, as suggested by the increased activity of both MGS (29) and DGS (32) in the presence of lipids with large negative J_s. This picture leads to a biophysical, intrinsic mechanism for MGS and DGS to control lipid biosynthesis as a function of the average monolayer spontaneous curvature of the membrane. Our model is a mathematical formulation of these ideas.

Cellular model of lipid biosynthesis

The biochemical constituents of our cellular model of lipid biosynthesis are the membrane lipids, the lipid biosynthetic enzymes, and the soluble cytoplasmic reactants. The membrane lipids are assumed to be homogenously distributed over both monolayers of the plasma membrane. Although labeling studies in *E. coli* show that lipid biosynthesis occurs mainly at the inner leaflet of the plasma membrane (33), we will assume that lipid transport from the inner to the outer leaflet of the membrane maintains a symmetric bilayer. Our assumption of spatial homogeneity for the lipids is based on the fast lateral diffusion of lipids in bilayers (34,35) and leads to a description in terms of ordinary differential equations. The soluble reactants (such as the nucleotide CTP or the inorganic phosphate ions P_i and PP_i) are assumed to have

TABLE 1 Spontaneous curvature and lipid composition of *A. laidlawii* grown in oleic acid

Lipid	PA	CDP-DAG	PGP	PG	DAG	MGlcDAG	DGlcDAG	GPDGlcDAG
J_s (nm^{-1})	−1/4.3	0	0	−1/8.7	−1/1.01	−1/2.5	−1/13.1	−1/7.7
Reference	(67)	*	*	(66)	(39)	(18)	(18)	*
$\mathbf{L_{exp}}$ (mol %)	0.7†	0.04†	0.04†	15.1	0.7†	7.8	54.4	21.2

*These J_s values are estimated. See Appendix A for a discussion.
†These lipid molar fractions were below the detection limit and are estimated. See Appendix A.

constant, regulated cytoplasmic concentrations, due to their involvement in general cellular processes. Therefore, they are only parameters (not variables) of the model.

The *A. laidlawii* lipid biosynthetic network is modeled as a system of nonlinear differential equations for eight lipids with seven enzymatic reactions. The variables of the model are compiled into the vector of lipid surface concentrations expressed in molar fraction: $\mathbf{L}^T = [\{PA\}\ \{CDP\text{-}PAG\}\ \{PGP\}\ \{PG\}\ \{DAG\}\ \{MGlcDAG\}\ \{DGlcDAG\}\ \{GPDGlcDAG\}]$. The sum of the lipid molar fractions is 1 at all times: $\mathbf{1}^T\mathbf{L} = 1$.

Each enzymatic reaction has a nonlinear rate equation of the Michaelis-Menten type, modified using surface dilution kinetics, as explained below, to account for the fact that the reactions take place on the membrane. The enzyme rate equations are compiled into a vector $\mathbf{v}^T = [v_{CDS}\ v_{PGPS}\ v_{PGPP}\ v_{PAP}\ v_{MGS}\ v_{DGS}\ v_{GPDGS}]$. The modulation of the enzyme activity due to the biophysical interaction with the mechanical properties of the membrane is introduced through a diagonal matrix $K_a = \mathrm{diag}([K_{a,CDS}\ K_{a,PGPS}\ K_{a,PGPP}\ K_{a,PAP}\ K_{a,MGS}\ K_{a,DGS}\ K_{a,GPDGS}])$, which incorporates the possibility that some of the enzymatic rates, specifically those of MGS and DGS, could depend on J_s^{mix}. If the enzyme is curvature sensitive, its association constant $K_{a,Enzyme}$ will depend on J_s^{mix}. Otherwise, the corresponding $K_{a,Enzyme} = 1$. This is the basis of the biophysical feedback mechanism, which will be introduced in the following section.

The topology of the reaction network is encoded in a stoichiometric matrix N, where N_{ij} is the number of lipid species i consumed (negative) or produced (positive) in reaction j:

$$N = \begin{pmatrix} -1 & 0 & 0 & -1 & 0 & 0 & 0 \\ 1 & -1 & 0 & 0 & 0 & 0 & 0 \\ 0 & 1 & -1 & 0 & 0 & 0 & 0 \\ 0 & 0 & 1 & 0 & 0 & 0 & -1 \\ 0 & 0 & 0 & 1 & -1 & 0 & 1 \\ 0 & 0 & 0 & 0 & 1 & -1 & 0 \\ 0 & 0 & 0 & 0 & 0 & 1 & -1 \\ 0 & 0 & 0 & 0 & 0 & 0 & 1 \end{pmatrix}.$$

The matrix N accounts for the enzymatic reactions and ensures mass conservation. However, our cellular model must also include both the lipid degradation into soluble products and the lipid insertion that enables a growing cell to double the number of lipids before cell division. These processes are incorporated through the transport vector $\mathbf{t}$ and the normalization vector $\mathbf{n}$. The transport vector $\mathbf{t}$ encapsulates the balance of lipids inserted and extracted. In our model, only PA is inserted at a constant cellular rate $V_{+,PA}$ and lipid degradation is assumed not to play a significant role in *A. laidlawii* lipid metabolism (36). Therefore, $\mathbf{t}^T = [V_{+,PA}\ 0\ 0\ 0\ 0\ 0\ 0\ 0]$.

The normalization vector $\mathbf{n}$, given by

$$\mathbf{n} = -(\mathbf{1}^T\mathbf{t})\mathbf{L},$$

reduces the surface concentration of each lipid in proportion to its molar fraction while at the same time maintaining the sum of the molar fractions equal to 1.

Combining all the terms, the model can be written compactly as

$$\frac{d\mathbf{L}}{dt} = NK_a(J_s^{mix})\mathbf{v}(\mathbf{L}) + \mathbf{t} + \mathbf{n}. \quad (1)$$

This system has stationary points $\mathbf{L}^*$.

Finally, to close the system, we need to relate J_s^{mix} to the lipid concentration. Our underlying, linear assumption is that J_s^{mix} is well approximated by the weighted average of the spontaneous curvatures of the individual lipids:

$$J_s^{mix} = \mathbf{J}_s^T\mathbf{L}. \quad (2)$$

This linear assumption has been shown experimentally to lead to an accurate approximation of the phase behavior of lipid mixtures (37). This linear assumption is also used in many of the experiments that measure the J_s of neutral and anionic lipids (38–41). Using Eq. 2 with the J_s values and experimental lipid composition $\mathbf{L_{exp}}$ in Table 1 leads to a calculated J_s^{mix} of $-1/7.9\ nm^{-1}$, which lies within the measured range from $-1/6.6\ nm^{-1}$ to $-1/8.1\ nm^{-1}$ of *A. laidlawii* lipid extracts.

Functional form of the lipid biosynthetic enzyme kinetic rates, v(L)

Before considering the biophysical mechanism that couples the biochemical reactions to the mechanical properties of the membrane, we state first some specific features of the enzyme kinetic rate equations of the membrane lipid network. The functional form of the rate equations $\mathbf{v}(\mathbf{L})$ in the model differs from standard enzyme kinetics (42) in two respects. First, our cellular model must take into account the number of copies of the enzyme in the cell. Second, we must account for the fact

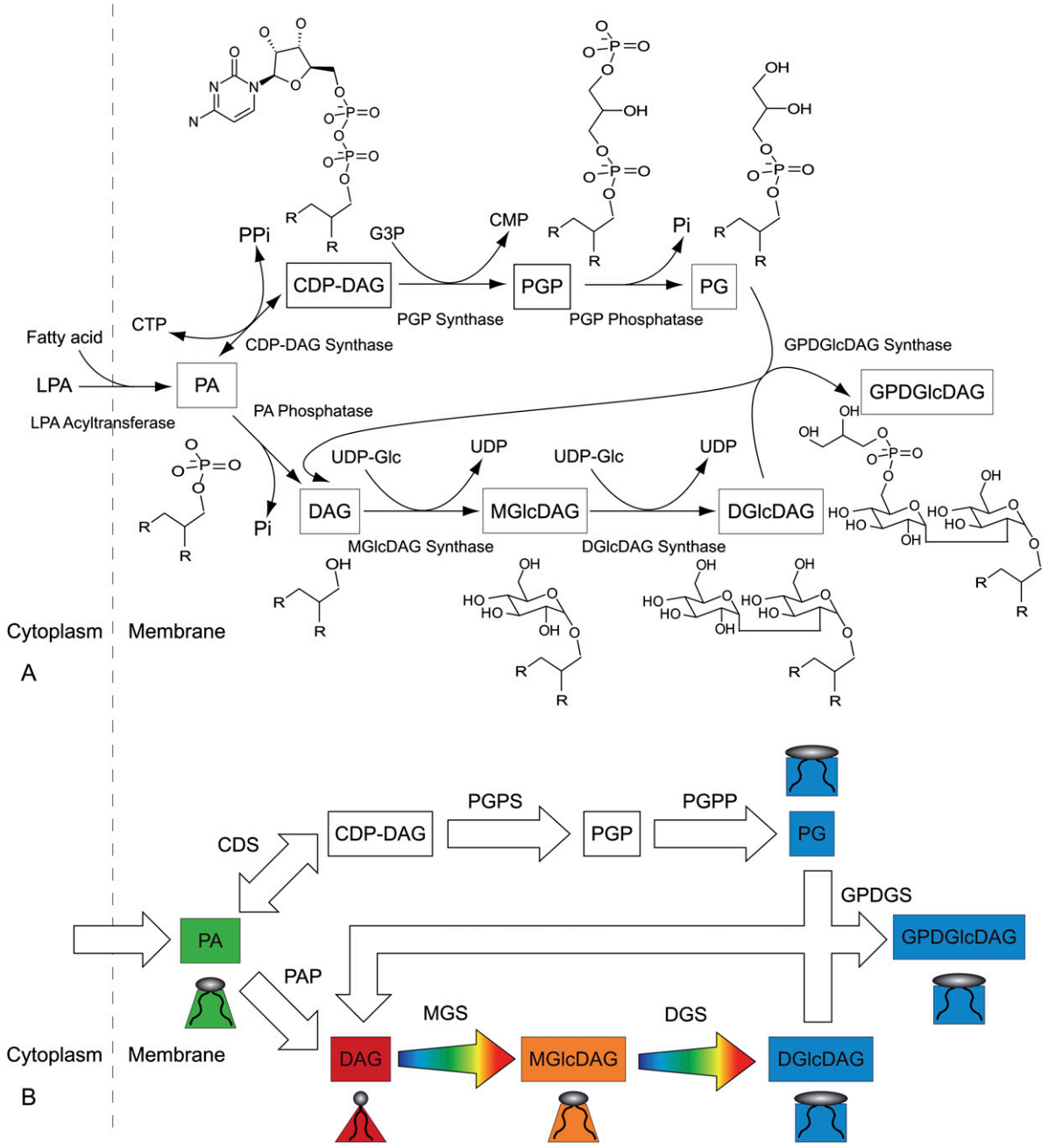

FIGURE 2 *A. laidlawii* lipid biosynthetic network. (*A*) The biochemical network. The main lipids in the plasma membrane of *A. laidlawii* A-EF22 are (6): phosphatidylglycerol (PG), diacylglycerol (DAG), monoglucosyl-DAG (MGlcDAG), diglucosyl-DAG (DGlcDAG), and glycerophosphoryl-DGlcDAG (GPDGlcDAG). Phosphatidic acid (PA), the liponuleotide CDP-DAG, and PG-phosphate (PGP) are lipid intermediates. The top branch is the PG pathway and the bottom branch is the glucolipid pathway. The abbreviated soluble reactants are glucose (Glc) and UDP-Glc, glycerol-3-phosphate (G3P), the inorganic phosphate ions P_i and PP_i, and the nucleotide CTP. *R* indicates an acyl chain. Six of the seven enzymes have irreversible rate equations. *A. laidlawii* also synthesizes three monoacyl derivatives of the glucolipids: monoacyl-MGlcDAG (MAMGlcDAG), monoacyl-DGlcDAG (MADGlcDAG), and monoacyl-bisglycerophosphoryl-DGlcDAG (MABGPDGlcDAG) (6). However, these lipids have been excluded from the model as they are not always synthesized (5) and their biosynthetic pathways have been postulated, but are not known (59). (*B*) A biophysical picture of the network. Lipids are color coded according to their J_s, which is linked to their molecular shape as shown. The same color code is used to show that the activity of MGS and DGS increases when the plasma membrane has a large negative J_s^{mix}. It can be seen, for instance, that in the case of the lower pathway the effect of MGS and DGS is to increase the effective size of the headgroup of the lipid upon which they are acting and therefore systematically increase the value of J_s among DAG, MGlcDAG, and DGlcDAG. By controlling the rate of the steps between DAG/MGlcDAG and MGlcDAG/DGlcDAG, the system is capable of regulating J_s^{mix}. *A. laidlawii* also synthesizes three monoacyl-derivatives of the glucolipids: monoacyl-MGlcDAG (MAMGlcDAG), monoacyl-DGlcDAG (MADGlcDAG), and monoacyl-bisglycerophosphoryl-DGlcDAG (MABGPDGlcDAG) (6). However, these lipids have been excluded from the model as they are not always synthesized (5) and their biosynthetic pathways have been postulated, but are not known (59).

that lipid biosynthetic enzymes have soluble, cytoplasmic reactants that diffuse in three dimensions, whereas their lipid reactants diffuse within the two-dimensional membrane.

Kinetic studies (27–29) have fitted the rates of *A. laidlawii* lipid biosynthetic enzymes to surface-dilution kinetics, in which soluble reactants have a bulk concentration in units of molarity and membrane reactants have a surface concentration in (dimensionless) molar fraction (43). All of the enzymatic reactions in the network, except for the reaction catalyzed by CDS, can be assumed to be irreversible. There is experimental evidence that supports this assumption, e.g., the hydrolyses of the phosphoanhydride bonds in PA and PGP are irreversible (44). Therefore, the rate equations for v_{PGPS}, v_{PGPP}, v_{PAP}, v_{MGS}, and v_{DGS} are of the form

$$\upsilon_{\mathrm{Enzyme}} = V_{\mathrm{cell}} \frac{\frac{\{L\}_{\mathrm{i}}}{K_{\mathrm{mL}}}\frac{[S]}{K_{\mathrm{mS}}}}{1+\frac{\{L\}_{\mathrm{i}}}{K_{\mathrm{mL}}}+\frac{[S]}{K_{\mathrm{mS}}}}, \tag{3}$$

where $\{L\}_{\mathrm{i}}$ is the surface concentration of the lipid substrate (in molar fraction) and $[S]$ is the bulk concentration of the soluble substrate (in units of molarity). Similarly, K_{mL} is the Michaelis constant of $\{L\}_{\mathrm{i}}$ (in molar fraction) and K_{mS} is the Michaelis constant of $[S]$ (in units of molarity). Experimental values of the enzyme kinetic constants are listed in Appendix B.

Note that V_{cell} is the rate for all copies of the enzyme in the cell (in units of molar fraction/min):

$$V_{\mathrm{cell}} = \frac{M_{\mathrm{Enzyme}}}{N_{\mathrm{Lipid}}} V_{\mathrm{max}}, \tag{4}$$

where M_{Enzyme} is the total mass of each enzyme in the cell and N_{Lipid} is the number of moles of lipid in the cell. V_{max} is the standard Michaelis-Menten limiting rate, which typically has units of moles of product synthesized per milligrams of enzyme per minute (42). It is assumed that the ratio $M_{\mathrm{Enzyme}}/N_{\mathrm{Lipid}}$ is kept constant in a growing cell over the cell cycle. In Appendix B we show how we have estimated these parameters.

Two of the enzymatic reactions have slightly different functional forms. The final reaction of the lower path, catalyzed by GPDGS, although irreversible, involves two lipid substrates. As mentioned above, the CDS reaction is modeled reversibly since the equilibrium constant is much less than 1 (23). The rate equations of these reactions are listed in Appendix B.

Spontaneous-curvature-sensitive enzymes

We now introduce the terms in the model that describe how the activity of an enzyme with an amphipathic α-helix is modulated as a function of spontaneous curvature, which is in turn a function of the lipid composition. As mentioned above, there is extensive evidence that supports the theory that the activity and function of many proteins, both integral and peripheral, are regulated by the biophysical properties of biological membranes (10,35). Such phenomena differ markedly from specific protein-lipid interactions. Although our model deals with the binding of an amphipathic α-helix to the membrane, the mechanism could be extended to describe the binding of other amphipathic motifs to the membrane.

Enzyme kinetic studies have shown that lipids with large negative J_{s} increase the activity of both MGS (29) and DGS (32). MGS has an amphipathic α-helix between residues 67 and 85 (30,45), that shares 5 of its first 8 residues with an α-helix of the *E. coli* division-site-selection protein MinD (46) that targets heterologous proteins to the membrane (47). Since it has been shown that MGS (19,29), the MGS amphipathic α-helix (20), and the MinD amphipathic α-helix (48) all preferentially bind to membranes with large negative $J_{\mathrm{s}}^{\mathrm{mix}}$, we hypothesize that the curvature-sensitive activity of MGS is a result of the membrane binding of this α-helix.

Through surface plasmon resonance (SPR) experiments, it has been concluded that liposomes bind to MGS through a two-step process (19). The first binding step is independent of lipid composition and has a dissociation constant of ~10 nM. The second binding step has a large dependence on lipid composition, as its dissociation constant decreases from 10 mM to 100 nM when the liposomes have large negative $J_{\mathrm{s}}^{\mathrm{mix}}$ (19). Since liposomes with large $J_{\mathrm{s}}^{\mathrm{mix}}$ increase both the activity of MGS and the strength of the second binding step, it follows that MGS is only active after the second binding step.

Amphipathic peptides form random coils in solution. The first binding step corresponds to surface adhesion induced by the electrostatic attraction of exposed basic residues to acidic membrane lipids. The second, subsequent step is the insertion of the hydrophobic residues into the membrane coupled with the emergence of the α-helix, which is entropically favored by the hydrophobic membrane environment. This two-step membrane binding (49) can be summarized through a simple kinetic mechanism,

$$Soluble \overset{K_{\mathrm{d1}}}{\rightleftharpoons} Surface \overset{K_{\mathrm{d2}}}{\rightleftharpoons} Inserted,$$

where K_{d1} and K_{d2} are the dissociation constants of the binding steps. At steady state, the fraction of membrane-inserted amphipathic α-helices that result in active enzymes is given by the association constant

$$K_{\mathrm{a}} = \frac{1}{1+K_{\mathrm{d2}}+K_{\mathrm{d1}}K_{\mathrm{d2}}}. \tag{5}$$

We now derive expressions for K_{d1} and K_{d2} from biophysical considerations.

First binding step, K_{d1}

From SPR studies, K_{d1} is measured to be ~10 nM (19). It is proposed that this first (irreversible) binding is a result of electrostatic attraction. Structurally, the presence of eight

positively charged residues on the 19-residue amphipathic α-helix (see Fig. 4 *B*) will produce a strong electrostatic attraction. Indeed, there is ample evidence that negatively charged anionic lipids are essential for the binding and activity of MGS. For instance, it is known that shielding the anionic lipids with 0.75 M NaCl prevents the binding of MGS (19).

From simple electrostatic considerations, K_{d1} is given by the Boltzmann relation,

$$K_{d1} = \exp\left(\frac{z_p e \psi_0}{k_B T}\right), \tag{6}$$

where $z_p e = +8e$ is the net charge of the amphipathic α-helix and ψ_0 is the membrane surface potential. A dissociation constant of 10 nM would imply $\psi_0 \cong -60$ mV at 40°C, which is comparable to the measured membrane surface potentials of bacterial lipid bilayers (50). This simple estimate reinforces the plausibility of the interpretation of the first binding step in terms of electrostatic interactions. Clearly, the biophysical picture will be complex, including the shielding of charges on the peptide to give an effective valence (51) and the likely involvement of other positively charged enzyme domains.

Second binding step, K_{d2}

The second binding step involves at least three energetic processes: membrane insertion of the hydrophobic residues; peptide folding to form the α-helix; and lipids bending to accommodate the inserted α-helix. It has been observed that K_{d2} decreases dramatically along the lipid sequence dioleoylphosphatidylglycerol (DOPG) > cardiolipin (CL) > dioleoylphosphatidylethanolamine (DOPE) > dioleoylglycerol (DOG) (19), i.e., as J_s becomes more negative (39,52). This is the basis for our assumption that the second binding step is dominated by the energy of lipids bending to accommodate the helix.

We can understand this process through the following simplified biophysical picture. Consider a locally flat bilayer with average monolayer spontaneous curvature J_s^{mix}. The diameter of the α-helix is comparable to that of a lipid. Consequently, the insertion of an amphipathic α-helix into a flat membrane does not result in a change of the monolayer curvature, yet it leads to a change in the molecular shape of the lipids alongside the α-helix (12) (Fig. 3 *A*). This would translate into a monolayer curvature, $c_{bound} \neq 0$, for a monolayer formed entirely by lipids like those surrounding the amphipathic α-helix.

Fig. 3 *A* sketches a very simple geometrical argument to obtain a first-order estimate of c_{bound}:

$$c_{bound} = -1/R_{bound} = \frac{-r}{\sqrt{A(r^2 + t^2)}}, \tag{7}$$

where $r = 0.45$ nm is the radius of the α-helix (53); t is the monolayer thickness (the distance between the middle of the α-helix and the bilayer midpoint), which is measured to be 1.71 nm (53); and A is the average interfacial surface area of the *A. laidlawii* lipids, which is measured to be 0.65 nm^2 (5). A is assumed to be square and the pivotal plane is assumed to coincide with the middle of the α-helix. Equation 7 gives an estimated $c_{bound} \approx -1/3.2$ nm^{-1}, which is significantly nonflat.

The cylindrical deformation of the α-helix ensures that one of the principal curvatures is zero, $c_2 = 0$. Therefore, the change in the stored elastic energy in Eq. 1 due to the bending of the lipids alongside the amphipathic α-helix is

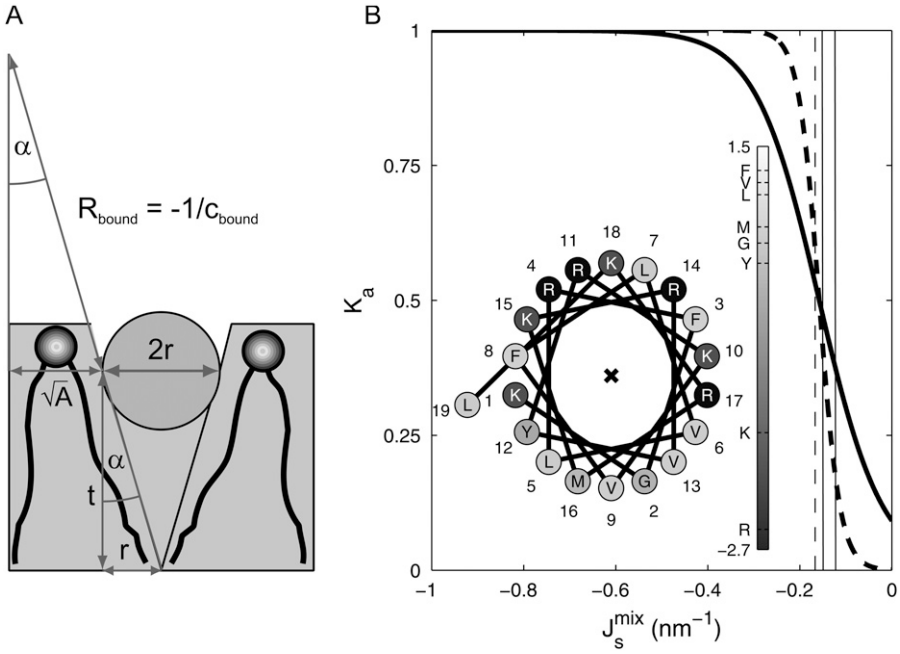

FIGURE 3 (*A*) Geometric argument used to calculate c_{bound}, the curvature of a lipid monolayer consisting entirely of lipids that lie alongside an amphipathic α-helix. (*B*) Association constant K_a as a function of J_s^{mix} for a 19-residue α-helix (*dark solid line*) and, for a 58-residue α-helix, such as that of CCT, plotted for comparison (*dark dashed line*). The dashed vertical line is $J_s = -1/6$ nm^{-1} and the solid vertical lines give the measured range of J_s^{mix} of lipid extracts (5). (*Inset*) Helical-wheel projection of residues 67–85 of MGS. The bar gives the Eisenberg consensus normalized hydrophobicity scale (76).

$$F(c_1 = c_{\text{bound}}) - F(c_1 = 0) = N_h A \frac{\kappa_M}{2} c_{\text{bound}}(c_{\text{bound}} - 2J_s^{\text{mix}}), \quad (8)$$

where κ_M is the bending rigidity of lipids, which we take to be 10 k_BT (38), and $N_h = 7.1$ is the number of lipids that adopt curvature c_{bound} along both sides of the amphipathic α-helix. N_h is calculated for a 19-residue α-helix of length 2.85 nm with 3.5 lipids of length $0.65^{1/2}$ nm along each side of its long axis. For the range of J_s values in Table 1, the free energy is between -1.7 k_BT/lipid and 0.2 k_BT/lipid. These energies are not large enough to cause the lateral sequestration of lipids around the α-helix (54), thus justifying the use of J_s^{mix}.

Equation 9 provides an estimate for the binding energy if we assume that the main energetic contribution to this process comes from lipid bending. The dissociation constant of the second binding step would then be given by the Boltzmann relation:

$$K_{d2} = \exp\left(N_h A \frac{\kappa_M}{2} c_{\text{bound}}(c_{\text{bound}} - 2J_s^{\text{mix}})/k_BT\right). \quad (9)$$

Note that for the range of J_s values in Table 1, the modeled K_{D2} ranges between 4 M and 5 μM. The difference with the experimental values of K_{D2} may be explained by the enhanced electrostatic attraction due to the absence of divalent cations and the use of zwitterionic lipids in the SPR experiments (19,20). Note that when $J_s^{\text{mix}} = c_{\text{bound}}/2 = -1/6.3$ nm^{-1}, the binding energy is zero and MGS is equally likely to be bound or unbound. Reassuringly, this bound-to-unbound transition is centered at a value of J_s^{mix} that lies between the formation of nonbilayer structures and the lower bound of the experimental curvature of lipid extracts in *A. laidlawii*: $-1/6 < c_{\text{bound}}/2 < -1/6.6$ (Table 1).

Equations 6 and 9 provide the biophysical feedback for the system in Eq. 1, as the association constant $K_{a,\text{MGS}}$ multiplies the rate v_{MGS}. Given the individual lipid spontaneous curvatures J_s in the system (Table 1), and assuming a constant $K_{d1} = 10$ nM, the association constant is constrained to be in the range $1 \geq K_{a,\text{MGS}} \geq 0.23$ (Fig. 3 *B*), and the 19-residue α-helix provides a fourfold regulation of MGS activity. At large negative J_s^{mix}, almost all MGS is active and the synthesis of MGlcDAG increases J_s^{mix}. The opposite effect is produced when J_s^{mix} is less negative. Clearly, a longer amphipathic α-helix would produce significantly stronger regulation of activity (Fig. 3 *B*).

Parameter estimation for the model

The time evolution of the system in Eq. 1 and its corresponding stationary point depend on the model parameters. Most of these parameters have been collected from an extensive survey of the literature, or have been estimated or measured directly. As is usual in the literature, some of the parameters carry substantial uncertainty. In addition, there is an absence of kinetic parameters for some of the enzymes of the *A. laidlawii* lipid biosynthetic network.

To complete our parametric description, we carry out a constrained nonlinear parameter estimation in which we search for the positive parameter set $\mathbf{p}$ that reproduces the experimentally observed lipid concentrations $\mathbf{L_{exp}}$ as close as possible while minimizing the distance to the reliable literature values. Our method of choice to solve this constrained optimization is the Stochastic Ranking Evolutionary Strategy (SRES) (55), an evolutionary strategy with stochastic ranking, which has been shown in a recent survey (56) to be successful in finding feasible parameters in nonlinear biochemical pathways.

For such an underdetermined system, a multiobjective optimization is pursued. The primary objective is to minimize the difference between $\mathbf{L^*(p)}$, the stationary point of the model in Eq. 1 for the parameter set $\mathbf{p}$, and the experimentally observed lipid composition $\mathbf{L}_{\text{exp}}$ given in Table 1,

$$\|\mathbf{L}^*(\text{p}) - \mathbf{L}_{\text{exp}}\|^2.$$

The secondary objective is to minimize the difference between the estimated parameter set $\mathbf{p}$ and the literature parameters $\mathbf{p}_{\text{lit}}$. Instead of minimizing the Euclidean norm $\|\mathbf{p} - \mathbf{p}_{\text{lit}}\|$, in our case we minimize a more appropriate measure of the relative distance between the parameter sets, previously introduced to quantify the robustness of dynamical systems (57),

$$\sum_j c_j \left|\log_{10}\left(\frac{p_j}{p_{\text{lit}_j}}\right)\right|,$$

i.e., the sum of the absolute logarithmic errors between $\mathbf{p}$ and $\mathbf{p}_{\text{lit}}$ weighted by c_j, the confidence in the jth literature parameter. In particular, parameters obtained from *A. laidlawii* experiments have been assigned $c_j = 1$, whereas $c_j = 1/2$ for parameters taken from experiments on other organisms, such as *E. coli*. As a check that the combination of our model and this multiobjective estimation procedure produces plausible parameter sets, we have verified that we can obtain parameters for which the model reproduces all the different lipid compositions that have been observed experimentally (5).

There are a total of 25 kinetic parameters in the model, of which only 18 have literature values. We run our multiobjective optimization by varying 15 parameters (the 7 unknown and 8 parameters with uncertain literature values) and obtain the estimated parameter set $\mathbf{p_0}$ presented in Table 2. The distance between each estimated parameter and its literature value has been constrained to be at most two orders of magnitude. The estimated parameter set reflects the sensitivity of the steady state to particular parameters, specifically those appearing in the numerator of the rate equations: $V_{\text{cell,Enzyme}}$ and the soluble substrate concentrations. This emphasizes the importance of measuring intracellular metabolite concentrations.

Our model in Eq. 1 with the estimated parameter set $\mathbf{p_0}$ in Table 2 will be our reference system henceforth. This system has a stationary point at the experimental lipid composition

TABLE 2 Model parameters for the reference system

Parameter	Literature (p_{lit})	Estimated (p_0)
$V_{+,PA}$, min^{-1}	8.2×10^{-3}	
$V_{cell,CDS}$, min^{-1} †	9.6×10^{-3}	
$V_{cell,PGPS}$, min^{-1} †	4.7×10^{-3}	
$V_{cell,PGPP}$, min^{-1}	*	3.2
$V_{cell,PAP}$, min^{-1}	4.1×10^{-2}	7.7×10^{-2}
$V_{cell,MGS}$, min^{-1}	1.8×10^{-3}	1.4×10^{-2}
$V_{cell,DGS}$, min^{-1}	3.5×10^{-4}	1.2×10^{-3}
$V_{cell,GPDGS}$, min^{-1}	*	1.5×10^{-2}
CDS $K_{M,PA}$, mol %	*	9.3×10^{-2}
PGPS $K_{M,CDPDAG}$, mol %	*	1.0×10^{-2}
PGPP $K_{M,PGP}$, mol %	*	38.2
PAP $K_{M,PGP}$, mol %	10	
MGS $K_{M,DAG}$, mol %	6	5.2
DGS $K_{M,MGlcDAG}$, mol %	1	
GPDGS $K_{M,PG}$, mol %	*	25
GPDGS $K_{M,DGlcDAG}$, mol %	*	85
CDS $K_{M,CTP}$, mM†	0.58	
PGPS $K_{M,G3P}$, mM†	0.32	
MGS $K_{M,UDP\text{-}Glc}$, mM	0.4	
DGS $K_{M,UDP\text{-}Glc}$, mM	0.14	
CDS K_{eqm}	0.22	
CTP, mM	0.5	
UDP-Glc, mM†	0.4	2.5
PP_i, mM†	1	
G3P, mM†	0.2	0.32

Parameters are obtained through a multiobjective optimization using the evolutionary algorithm SRES (55). Parameters marked * have not been measured. Parameters marked † correspond to *E. coli* and are given less weight in the optimization. See Appendix B for references and details of the literature parameters.

shown in Table 1, with $J_s^{mix} = -1/7.9\,nm^{-1}$. In the next section, we explore the effect of the biophysical regulation mechanism introduced above.

RESULTS

We now investigate the behavior of the cellular model of lipid biosynthesis through the numerical integration of Eq. 1 under a variety of conditions. The first robust feature of the model is that it evolves to a steady state that is independent of the initial condition. Although we have not proved global stability explicitly, numerical integrations from more than 10^5 randomly generated initial conditions all converge to the same stationary lipid composition. This is strong evidence that the steady state is globally attracting. Our numerical investigation of the model therefore translates into an evaluation of how the fixed point $\mathbf{L}^*(\mathbf{p})$ changes in response to variations in the parameters or in the presence of feedback.

Which enzyme rates most affect J_s^{mix}?

Experiments indicating that the activities of both MGS and DGS are curvature-sensitive (28,29) have led to the hypothesis that these two enzymes are responsible for the control of J_s^{mix}. If this is true, the rates of MGS and DGS must have a large effect on the steady-state $J_s^{mix}(\mathbf{L}^*)$. In this section, we use our model to determine which enzymes of the *A. laidlawii* lipid biosynthetic network have the largest effect on $J_s^{mix}(\mathbf{L}^*)$ in the absence of feedback. This is an initial step before we introduce the biophysical feedback explicitly in the next section, i.e., in this section the matrix K_a does not depend on the curvature J_s^{mix}.

This question can be posed in the well-known framework of sensitivity analysis, which has been used to characterize, *e.g.*, the robustness of bacterial chemotaxis networks (57). For the reference parameters $\mathbf{p_0}$ (Table 2), the model evolves to the experimental lipid composition $\mathbf{L_{exp}}$ (Table 1), i.e., $\mathbf{L}^*(\mathbf{p_0}) = \mathbf{L_{exp}}$. However, the parameters $\mathbf{p}$ are inherently noisy. Specifically, the seven $V_{cell,Enzyme}$ have the most influence on the steady state while at the same time having large variability. Therefore, our sensitivity analysis investigates how changes in the different $V_{cell,Enzyme}$ translate into variations of the steady-state $J_s^{mix}(\mathbf{L}^*)$.

The sensitivity analysis is performed through Monte Carlo sampling, one enzyme at a time. The $V_{cell,Enzyme}$ of the enzyme under study is fixed at the reference value in Table 2. We then produce 10^6 parameter sets where the other six $V_{cell,Enzyme}$ are drawn from a random distribution conditioned to produce uniform sampling (over the interval [0,6]) of the logarithmic variation of the parameter set, k:

$$k = \sum_j \left| \log_{10}\left(\frac{p_j}{p_{0j}}\right) \right|. \quad (10)$$

Clearly, this implies that the individual $V_{cell,Enzyme}$ parameters are not sampled uniformly (see the *inset* of Fig. 4 *A*). Effectively, our sensitivity analysis considers variations of up to almost two orders of magnitude in each of the six $V_{cell,Enzyme}$, and an overall uniform variation of six orders of magnitude for the complete parameter set. The fixed point for each of the 10^6 parameter sets is obtained and the corresponding J_s^{mix} is calculated.

Fig. 4 *A* shows the results for the enzyme MGS as a two-dimensional histogram of $P_{MGS}(J_s^{mix}, k)$, the distribution of the 10^6 random parameter sets. As expected, the distribution is centered on the reference value of $J_s^{mix} = -1/7.9\,nm^{-1}$ and becomes broader as the variation of the parameter set, k, grows. Since biophysical experiments show that membranes with $J_s^{mix} < -1/6\,nm^{-1}$ do not form bilayers, we can consider such compositions as biologically nonviable (17). This is marked as a dashed line in Fig. 4 *A*. Therefore, the distribution $P(J_s^{mix}, k)$, or its marginal $P(J_s^{mix})$, quantifies how likely it is for the system to evolve to a nonbilayer state when a particular enzyme is kept fixed at its reference value and all other enzymes have uncertain $V_{cell,Enzyme}$ values. Essentially, this is also a measure of the relevance of the particular enzyme for the controllability of the system, as it quantifies the variability of the output when a given parameter is kept tightly controlled.

The complete results for the system are summarized in Fig. 4 *B*, where we plot the marginal distributions $P_{Enzyme}(J_s^{mix})$

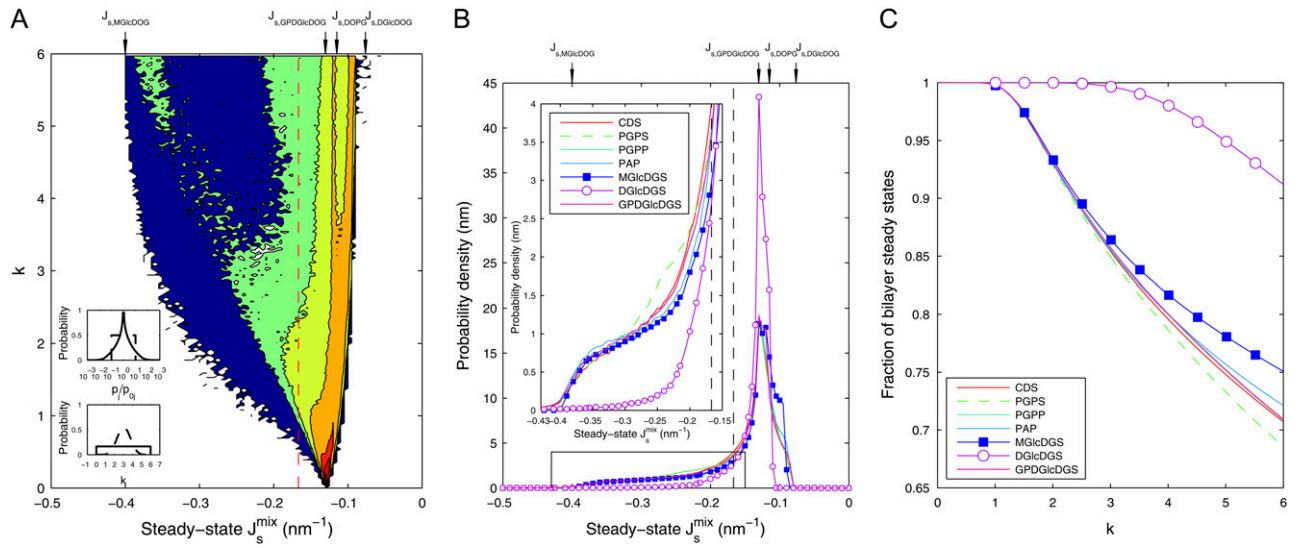

FIGURE 4 (*A*) Histogram of the distribution $P_{MGS}(J_s^{mix}, k)$ of the steady-state J_s^{mix} for a sampling of 10^6 random parameter sets, where $V_{cell,MGS}$ is fixed and the other six $V_{cell,Enzyme}$ values are varied. k is defined in Eq. 10 and measures the logarithmic variation of the parameter set. The individual $V_{cell,Enzyme}$ distribution used (*solid*, *top inset*) ensures that the logarithmic variation k is sampled uniformly (*solid*, *bottom inset*). If uniform individual $V_{cell,Enzyme}$ distributions were used (*dashed*, *top inset*), then k would approach a Gaussian distribution (*dashed*, *bottom inset*). (*B*) Marginal probability distributions $P_{Enzyme}(J_s^{mix})$ of all seven enzymes, where one $V_{cell,Enzyme}$ is fixed, whereas the other six $V_{cell,Enzyme}$ are varied. The dashed vertical line indicates the critical value $J_s^{mix} = -1/6\,nm^{-1}$ below which bilayers do not form. (*C*) Cumulative probability that the steady state will be viable ($J_s^{mix} > -1/6\,nm^{-1}$) against the logarithmic variation k of the state.

for the seven enzymes. All the distributions are centered on the reference J_s^{mix} value of $-1/7.9\ nm^{-1}$; however, the variance and the tails of the distributions differ. Specifically, DGS and MGS (marked with symbols in Fig. 4 *B*) have much smaller variances and sharper decay tails than the other five enzymes. The left tail of the distribution is relevant as it gives the proportion of biologically inviable stationary states that do not form bilayers. Fig. 4 *C* shows the fraction of viable steady-state lipid compositions as a function of the variability k. The results clearly show that keeping the rate of DGS fixed to its reference value is the most efficient way of guaranteeing a viable system.

The reason for this sensitivity is clear if we examine the network in Fig. 2 *B*. The enzyme DGS catalyzes the synthesis of DGlcDAG, with a small negative J_s, from MGlcDAG, with a large negative J_s. Since the membrane binding of amphipathic α-helices is increased by lipids with large negative J_s, this provides a direct link with the biophysical feedback mechanism described above. The implication is that enzymes that catalyze reactions that result in a large positive change in J_s^{mix} (i.e., DGS and to a lesser extent MGS) are strong candidates to exert the biophysical feedback control of membrane curvature, in accordance with kinetic data. In the next section, the effect of the biophysical feedback provided by the amphipathic motifs is investigated in detail.

Effect of the biophysical feedback on J_s^{mix}

We now study the effect of the biophysical feedback, mediated by amphipathic α-helices, on the control of the steady-state J_s^{mix}. Our model encodes this mechanism through the association constants $K_{a,MGS}$ and $K_{a,DGS}$ collected in the matrix $K_a(J_s^{mix})$.

A sensitivity analysis similar to that performed in the preceding section is carried out to measure how much the variability of the system is reduced in the presence of feedback. We draw 10^6 parameter sets from a random distribution of $V_{cell,Enzyme}$ such that the logarithmic variation k, defined in Eq. 10, is uniform over the interval [0,7]. Fig. 5 *A* shows four marginal distributions of the steady-state J_s^{mix} of the system without feedback and with different combinations of feedback on MGS and DGS. In particular, we model MGS to have a 19-residue amphipathic α-helix (see Fig. 3 *B*) and we hypothesize that a similar α-helix is responsible for the curvature-sensitive activity of DGS, as suggested by secondary-structure predictions (30). The numerics show that the effect of feedback is noticeable in the reduction of the left tail of the distribution. This means that inviable, nonbilayer steady states are less probable when feedback is present. This is especially prominent for DGS, although MGS also contributes to the control of J_s^{mix}, as shown in Fig. 5 *B*. The combined feedback of MGS and DGS reduces the fraction of inviable oleoyl acyl lipid compositions by 19%.

The robustness of the lipid compositions

A central feature of the biophysical feedback mechanism is the fact that the enzymatic network controls the physical property J_s^{mix} and not the steady-state lipid concentrations $\mathbf{L}^*$. However, J_s^{mix} is a function of the lipid concentrations,

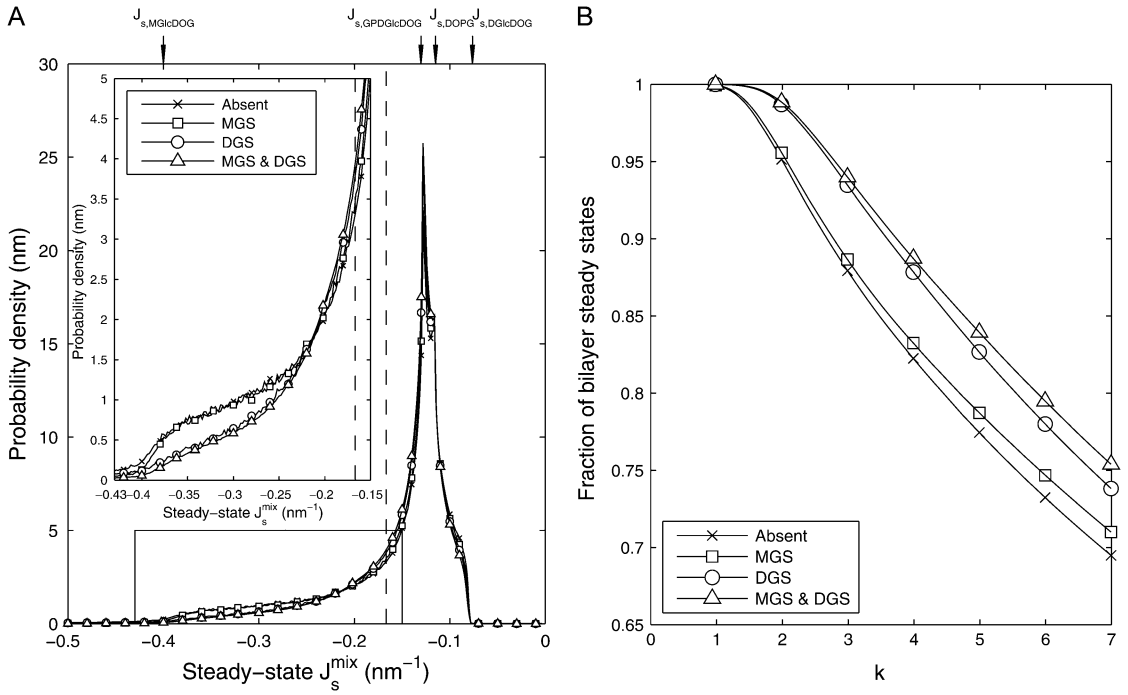

FIGURE 5 (*A*) Effect of the biophysical feedback on the control of the steady-state J_s^{mix}. The four marginal distributions $P(J_s^{mix})$, obtained from 10^6 random parameter sets in which all seven enzyme rates $V_{cell,Enzyme}$ are varied, show a reduction of the probability of inviable states with $J_s^{mix} < -1/6\ nm^{-1}$. In the absence of feedback, we fix $K_{a,MGS}$ at the reference value of $K_{a,MGS}$ ($J_s^{mix} = -1/7.9\,nm^{-1}$) shown in Fig. 3 *B* (×). MGS is modeled to have a 19-residue α-helix (□), DGS is modeled with a 19-residue α-helix (○), both MGS and DGS are modeled with 19-residue α-helices (△). (*B*) The cumulative probability that the steady state forms a bilayer ($J_s^{mix} > -1/6\,nm^{-1}$) as a function of the logarithmic variation k.

and it is important to study the underlying variability of **L***, with respect to the reference lipid composition $\mathbf{L_{exp}}$, when the parameters of the model are uncertain. This point can be illustrated with the data obtained in the preceding section through our sensitivity analysis. Fig. 6 shows the probability distribution of steady-state compositions **L*** as a function of J_s^{mix} and $\|\mathbf{L}^* - \mathbf{L_{exp}}\|_1$, the distance to the experimental lipid composition, in the absence and in the presence of feedback.

In the absence of feedback (Fig. 6 *A*), the data show that a majority of **L*** are close to $\mathbf{L_{exp}}$, but a range of lipid mixtures is allowed by the system. Note that the system does not by default evolve toward pure, monocomponent compositions. In addition, the **L*** in the biologically viable region ($J_s^{mix} > -1/6\,nm^{-1}$) consist mostly of mixtures of PG, DGlcDAG, and GPDGlcDAG, and not of the intermediates PA, CDP-DAG, or PGP. On the other hand, the inviable **L***, with $J_s^{mix} < -1/6\,nm^{-1}$, appear through the increase in MGlcDAG, and not of DAG. These trends stem from the constraints that the network structure imposes on the control mechanism and highlight how the steady-state J_s^{mix} is bounded by the simplex of the J_s values of the individual lipids.

Fig. 6 *B* shows that the most notable effect of the feedback is to reduce the likelihood of inviable states with values of $J_s^{mix} < -1/6\,nm^{-1}$, specifically those with high concentrations of MGlcDAG. In addition, our numerical results clearly indicate that the control is not achieved by targeting specific (possibly monocomponent) compositions, as the overall shape of the probability distribution remains broadly unchanged and mixed states are the norm. In fact, the proportion of monocomponent states is reduced when the feedback is on. Another effect of the feedback is the increase of the probability of states with J_s^{mix} close to the boundary between bilayer and nonbilayer states. This follows from the functional form of the feedback that is centered on the value $c_{bound}/2 = -1/6.3\,nm^{-1}$. This is clearly observable in Fig. 6. The implication is that lipid compositions with large negative J_s^{mix} are more improbable, but at the same time there is an increase in lipid compositions with J_s^{mix} close to the bilayer to nonbilayer transition.

The effect of the length of the amphipathic α-helices

As seen in Fig. 3 *B*, the proposed biophysical feedback exerted by a 19-residue amphipathic α-helix gives rise to a fourfold regulation, which results in a modest reduction of the likelihood of inviable states. The functional form of our feedback implies that the magnitude of the feedback depends strongly on the length of the amphipathic α-helix. We now investigate how the length and number of amphipathic α-helices on MGS and DGS affect J_s^{mix} regulation.

Biological evidence indicates that the size of amphipathic motifs should be studied parametrically as it is an important

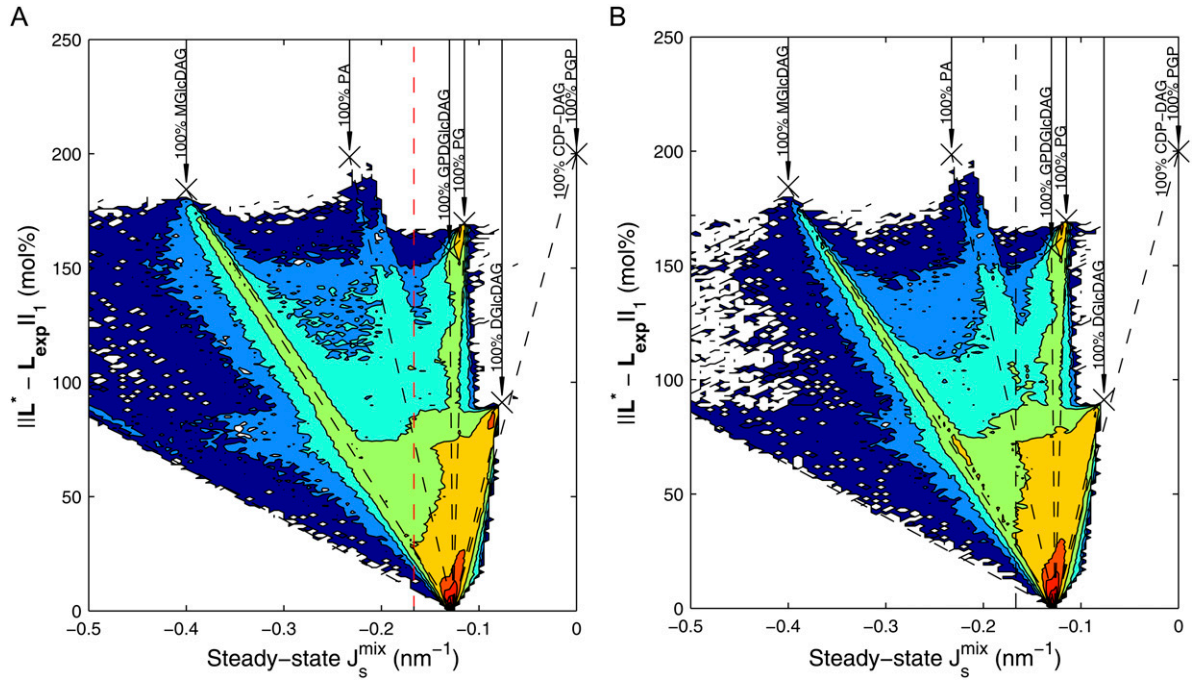

FIGURE 6 Histogram of the distribution of steady-states **L***, showing the probability distribution of J_s^{mix} and the distance of **L*** to the experimental concentration $\mathbf{L_{exp}}$. The data are obtained by sampling 10^6 random parameter sets as in Fig. 5. (*A*) Distribution in the absence of feedback. The vertical dashed line at $J_s^{mix} = -1/6\,nm^{-1}$ separates the nonbilayer and bilayer fractions. The dashed lines correspond to the steady-state J_s^{mix} that results from adding a particular lipid to $\mathbf{L_{exp}}$ until one reaches a monocomponent state, marked by crosses. (*B*) Distribution when both MGS and DGS exert biophysical feedback through a 19-residue amphipathic α-helix.

feature in protein-membrane interactions. Secondary-structure predictions suggest that both MGS and DGS have multiple α-helices that may insert into the membrane (20,30). However, it is difficult to identify amphipathic α-helices and determine their length from genetic sequences. It is also important to mention that some enzymes with amphipathic α-helices can act in concert. For instance, there is evidence that CCT acts as a dimer that is only active when the 58-residue amphipathic α-helices of both monomers are bound to the membrane (58). In a simplified picture, this dimer would be viewed as having an effective amphipathic α-helix of 116 residues.

Fig. 7 plots the dependence on the length of the amphipathic α-helices of the marginal distribution $P(J_s^{mix})$ in Fig. 5 *A*, where both MGS and DGS are curvature sensitive. Clearly, as the length of the α-helices is increased, the distribution becomes sharper and the likelihood of getting inviable states is reduced. As the inset of Fig. 7 shows, the reduction in the proportion of nonbilayer states increases to more than 50% when both MGS and DGS have 60-residue α-helices.

DISCUSSION

This article outlines a bottom-up modeling framework that couples a biochemical network with an intrinsic biophysical feedback mechanism. The central idea behind the biophysical regulation is that the activity of certain enzymes involved in lipid biosynthesis is dependent on the spontaneous curvature of the lipids, which is itself a function of the lipid composition. This introduces a feedback loop that can regulate J_s^{mix}, a property that must be kept within a narrow window to allow for cellular activity and survival (3,7).

The numerical results of our model show that the system evolves toward biologically plausible mixtures of lipids. When the biophysical regulation is present, it decreases the likelihood of inviable steady-state lipid compositions that would not be expected to form a lamellar bilayer. Moreover, our sensitivity analysis indicates that two enzymes in the network (DGS and MGS) have the largest effect on the steady-state J_s^{mix}, in agreement with kinetic data. This fact follows from both the intrinsic properties of the enzymatic reactions (the corresponding substrates have large negative J_s and the reactions result in large positive changes in J_s), and from their position in the lipid biosynthetic network. Therefore, the model underscores the possibility that a chemically nonspecific, biophysical mechanism can participate effectively in the regulation of J_s^{mix} in the plasma membrane. Such a mechanism implies that the lipid biosynthetic enzymes regulate the concentration of individual lipids not only as a function of their own concentration but also as a result of larger scale, mechanical properties of the membrane.

The sensitivity analysis used here brings to the fore the importance of characterizing parameter variability in biological systems. Indeed, the sensitivity of J_s^{mix} is dependent on

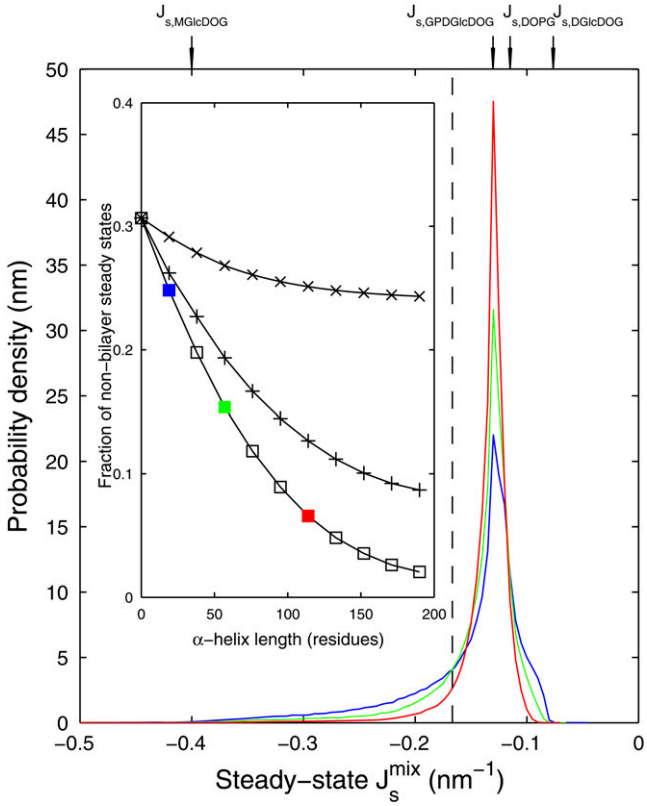

FIGURE 7 Effect of amphipathic α-helix length on steady-state J_s^{mix}. Shown are three marginal distributions $P(J_s^{mix})$ of the steady-state J_s^{mix} under uncertain parameters where both MGS and DGS are curvature sensitive with amphipathic α-helices of different lengths: 19-residue (*blue*, same as Fig. 5 *A*), 57-residue (*green*), and 114-residue (*red*). Vertical dashed line at $J_s^{mix} = -1/6\,nm^{-1}$ indicates the nonbilayer region. (*Inset*) Probability that the steady state does not form a bilayer against α-helix length, when MGS has an α-helix ($\times$); DGS has an α-helix ($+$); and MGS and DGS both have α-helices ($\square$). Colored squares correspond to the three plotted $P(J_s^{mix})$ in the main figure.

how the parameters are varied. In the absence of additional knowledge, our approach has been to sample the $V_{cell,Enzyme}$ parameter sets uniformly according to their relative logarithmic distance to the reference set, k, with a maximum variation for each individual parameter of $\sim$2 orders of magnitude. This leads to mixed steady-state lipid compositions localized mostly in the biologically viable region (Fig. 6). However, if the parameter variation is larger, our numerics indicate that monocomponent steady-state lipid compositions begin to appear. At present, it is difficult to infer from experimental results the range of $V_{cell,Enzyme}$ a cell is likely to experience and is likely to be robust to. For example, cells that overexpress enzymes 100 times are often still viable; however, this is unlikely to result in a 100-fold increase in enzyme activity. Clearly, the shape and width of the parameter distributions are an essential part of a meaningful sensitivity analysis of biological systems, and further experimental characterization in this area is needed.

Our study also highlights the importance of the length of the amphipathic α-helix as it is related (linearly in our simple model) to the energy released when it is inserted into the membrane. This suggests that the membrane binding of short amphipathic α-helices, such as the eight-residue α-helix on *E. coli* MinD (46), is less sensitive to J_s^{mix}, whereas the binding of long amphipathic α-helices is much more sensitive to J_s^{mix}. In addition, enzymes that act as oligomers provide more effective regulation of J_s^{mix}, as seems to be the case with CCT. This aspect of the influence of α-helix length on the regulation of J_s^{mix} could be investigated experimentally by site-directed mutagenesis.

The proposed modeling framework could be extended in several directions. First, our model has been constructed considering amphipathic α-helices at its core, with an estimate for the binding energy based on a simple geometric calculation of the curvature around an α-helix. This very simplified picture could be generalized to include entropic contributions and the possibility of more general amphipathic motifs (10). Such an extension would be incorporated into the association constant that encodes the regulation. Second, our model excludes the monoacyl (MA)-derivatives of the glucolipids: MAMGlcDAG, which is rarely present, and MADGlcDAG and MABGPDGlcDAG, which are each only present at $\sim$10 mol % when the lipids have a palmitoleoyl fraction $>$30 mol % (5). The model could be extended to include the MA-derivatives, although this would require a more detailed understanding of the postulated biosynthetic pathways (59). However, based on the insight provided by the current model, it is unlikely that the enzymes involved in the synthesis of MA-derivatives would have their activity modulated by amphipathic α-helices, since synthesis of these lipids would lead to a more negative $J_{s,mix}$.

Another extension would be to model the effect of lipid acyl chain length, which directly affects the J_s of a lipid, on the lipid composition (5,18,60). In its present form, the model only considers lipids with oleoyl acyl chains. However, Fig. 6 illustrates how important the individual lipid spontaneous curvatures are in determining the steady-state J_s^{mix}. Experimentally, it is known that if *A. laidlawii* is fed shorter and saturated fatty acids (making the J_s values in Table 1 more positive), the organism reacts by changing the proportion of lipid headgroups (5). The length and saturation of the lipid acyl chains have a nonlinear, but as yet unquantified, effect on the spontaneous curvature (39). The challenge is to model how the length and degree of unsaturation of the lipid acyl chains affect the lipid J_s values and to relate this to lipid biosynthesis. Based on our results, the acyl chain length will undoubtedly affect the regulatory role of MGS and DGS. When the lipids have shorter, saturated acyl chains, MGlcDAG and DAG are present at a significantly higher molar fraction. Since MGS catalyzes the reaction between these two lipids, it is hypothesized that when the lipids have shorter, saturated acyl chains, MGS will play a larger regulatory role.

The model can be used to study lipid biosynthesis in other organisms, but it would have to be extended to deal with the particular biochemical and biophysical characteristics of each network. In particular, it is likely that more lipid species will be present, thus increasing the dimensionality of the model and leading to diverse control strategies in different organisms. For instance, *E. coli* is known to regulate J_s^{mix} by changing the unsaturation of the lipid acyl chains (7). This results in a combinatorial increase in the number of chemical species and to a lesser extent the number of enzymes. In addition, a detailed understanding of the lipid-dependent activity of the enzymes that control the metabolism of lipid acyl chains would also be necessary. This does, however, highlight the importance of characterizing the biophysical properties of individual lipid types including the values of their monolayer spontaneous curvature. At present this is a relatively neglected area of research and this is a damaging oversight given the role of lipids in regulating key biological processes.

Finally, the connection of lipid biosynthesis to the cell cycle and the spatial inhomogeneity of lipids are two closely interconnected areas in which the modeling framework could be extended. Lipid biosynthesis is linked to the cell cycle by the need to double the lipid mass before cell division (61). Furthermore, experiments show that the anionic lipid cardiolipin (62) and peptides that contain amphipathic α-helices, such as MinD (63) and MGS (45), localize at the bacterial poles. This localization may act as a trigger for lipid biosynthesis and cell division. Experimental evidence also shows that bacterial membranes may exhibit transbilayer asymmetry (64) and may be divided into domains, for instance a septal and a polar region (62), which have vastly different lipid compositions and enzyme concentrations. In these cases, the modeling framework could be extended to model the lipid compositions in the different lipid domains and lipid monolayers separately.

APPENDIX A: LIPID COMPOSITIONS AND J_S VALUES (TABLE 1)

The lipid composition in Table 1 is Extract 13 from Andersson et al. (5). This lipid composition also contains 3.2 mol % of the monoacyl-DGlcDAG (MADGlcDAG), which we model as MGlcDAG in Table 1. The assumption is that the J_s of MADGlcDAG (2 glucose: 3 acyl chains) is close to that of MGlcDAG (1 glucose: 2 acyl chains). The molar fractions of DAG and the lipid intermediates, PA, CDP-DAG, and PGP, are often below the experimental detection limit. In our model, any unaccounted molar fraction is distributed among these lipids and we assume that PA and DAG are present at 20 times the level of CDP-DAG and PGP, based on *E. coli* data (65).

The J_s values of DOPG (66), dioleoylphosphatidic acid (DOPA) (67), and DOG (39) have been measured experimentally. The J_s values of DOPG and dioleoylphosphatidic acid are both taken from experiments with a divalent cation concentration above 20 mM. This reproduces the *A. laidlawii* cytoplasmic environment where a divalent cation is bound to 1 in 10 anionic lipids (68). The J_s values of MGlcDOG, DGlcDOG, and the *A. laidlawii* lipid extracts are estimated from the measured hexagonal phase cylinder diameter d (18), using the equation $J_s = 1/(d/2 - 0.9\ \text{nm})$. CDP-DAG and PGP are present at negligible amounts and their J_s values are estimated to be 0 nm^{-1}. The estimated spontaneous curvature of GPDGlcDOG follows from using the linear assumption in Eq. 2 and the experimental range of lipid extract J_s^{mix} values of between $-1/6.6\ nm^{-1}$ and $-1/8.1\ nm^{-1}$ to give a value of $J_s = -1/7.7\ nm^{-1}$. This estimated value suggests GPDGlcDAG forms a lipid bilayer and is consistent with observations that GPDGlcDAG, with a mixture of palmitoyl and oleoyl acyl chains, forms a mixture of micellar and lamellar aggregates (69). The J_s value of the anionic lipid GPDGlcDAG is also likely to depend on the concentration of free and bound cations (66). The lipid J_s values in Table 1 give a J_s^{mix} in the experimental range for all other measured oleoyl acyl lipid compositions (5,18).

TABLE 3 Enzyme kinetic constants

Enzyme	V_{max} (μmol mg^{-1} min^{-1})	K_{mL} (molar fraction)	K_{mS} (mM)	K_{eqm}	Reference
CDP-DAG synthase*	55	†	0.58	0.22	(23)
PGP synthase*	20	†	0.32	N/A	(24)
PA phosphatase	12.8	0.1	N/A	N/A	(27)
MGlcDAG synthase	12	0.08	0.4	N/A	(28)
DGlcDAG synthase	1.3	0.01	0.14	N/A	(29)

*V_{max} and K_m kinetic constants of these enzymes are taken from *E. coli*.
†These enzymes were not studied with the surface dilution mechanism.

APPENDIX B: LITERATURE MODEL PARAMETERS (TABLE 2)

Functional forms for v_{GPDGS} and v_{CDS}

Two reactions of the lipid biosynthetic network are not described by Eq. 3, which is an irreversible Michaelis-Menten kinetic rate equation with one lipid substrate and one soluble substrate. GPDGS catalyzes an irreversible reaction, but the reaction involves two lipid substrates. This gives a rate equation with the functional form,

$$v_{Enzyme} = V_{cell}\frac{\dfrac{\{L\}_i\{L\}_j}{K_{mL_i}K_{mL_j}}}{1+\dfrac{\{L\}_i}{K_{mL_i}}+\dfrac{\{L\}_j}{K_{mL_j}}}. \quad \text{(B1)}$$

The reaction catalyzed by CDS is reversible and is modeled with a reversible rate equation,

$$v_{Enzyme} = V_{cell}\frac{\dfrac{\{L\}_i[S]}{K_{mL}K_{mS}}\left(1-\dfrac{\{L\}_j[P]}{\{L\}_j[S]}\right)}{1+\dfrac{\{L\}_i}{K_{mL}}+\dfrac{[S]}{K_{mS}}+\dfrac{\{L\}_j}{K_{mL}}+\dfrac{[P]}{K_{mS}}}, \quad \text{(B2)}$$

TABLE 4 V_{cell}

Enzyme	Enzyme yield	$V_{cell,\ Enzyme}$ (min^{-1})	Reference
CDP-DAG synthase	1/8000*	9.6×10^{-3}	(23)
PGP synthase	1/6000*	4.7×10^{-3}	(24)
PA phosphatase	1/440	4.1×10^{-2}	(27)
MGlcDAG synthase	1/9100	1.8×10^{-3}	(28)
DGlcDAG synthase	1/5250	3.5×10^{-4}	(29)

*Enzyme yield of these enzymes is taken from *E. coli*.

TABLE 5 Soluble reactant concentrations

Reactant	Concentration (mM)	Reference
CTP	0.5	(72)
PP_i	6*	(73)
G3P	0.2*	(74)
UDP-glucose	0.4*	(75)

*These intracellular concentrations are not from *A. laidlawii*.

where $[P]$ is the soluble product bulk concentration; the lipid product and soluble product Michaelis constants are assumed to be equal to the substrate Michaelis constants K_{mL} and K_{mS}, respectively; and K_{eqm} is the equilibrium constant.

Enzyme kinetic constants

Three of the seven *A. laidlawii* lipid biosynthetic enzymes have been studied in detail. In addition, we use experimental data for two other reactions from *E. coli*. Although *E. coli* and *A. laidlawii* are very different organisms, most sequenced bacterial genomes are found to encode a protein that has a strong homology to CDP-DAG synthase of *E. coli* (22). Table 3 summarizes the corresponding V_{max}, K_{mL}, K_{mS}, and K_{eqm} values.

The V_{cell} values are obtained from Eq. 4 using the V_{max} in Table 3 and the ratio M_{Enzyme}/N_{Lipid} (protein mass to moles of lipid per cell), which is estimated as follows. *A. laidlawii* has 1.35 μmol of polar lipid for each milligram of membrane protein (70). Polar lipids constitute ~40% of the *A. laidlawii* membrane. Membrane proteins are measured to constitute 21.2% of the overall protein mass (71). This gives an $M_{Protein}/N_{Lipid}$ ratio of 1.4 mg μmol^{-1}. The enzyme yield $M_{Enzyme}/M_{Protein}$ is taken from the purification of each enzyme and is given in Table 4, which also presents the resulting estimate of V_{cell}.

Soluble reactant concentrations

The rate equations for the enzymatic reactions feature the soluble substrates G3P and uridine diphosphate (UDP)-glucose, CTP, and PP_i. In our model, we assume that the soluble metabolites are not dynamic variables and have the constant, regulated cytoplasmic concentrations in Table 5. This assumption is motivated by their involvement in many cellular processes other than lipid biosynthesis.

Lipid insertion

The enzyme that synthesizes PA in *A. laidlawii* is not well characterized. Therefore, $V_{+,PA}$ is estimated from the doubling time of *A. laidlawii*. In an exponentially growing membrane, the number of lipids is given by

$$N_{Lipid}(t) = N_{Lipid}(0)\exp(tV_{+,PA}). \quad \text{(B3)}$$

Taking the doubling time of *A. laidlawii* in the exponential growth phase to be between 80 and 90 min (Å. Wieslander, University of Stockholm personal communication, 2003, 2004), $V_{+,PA}$ is 8.2×10^{-3} min^{-1}.

The authors thank Åke Wieslander for providing invaluable expertise of the lipid biosynthesis of *A. laidlawii*. We also thank Robin Leatherbarrow for insightful discussion. We are grateful to Thomas P. Runarsson and Xin Yao for their SRES algorithm, which is available online.

REFERENCES

1. Ces, O., and X. Mulet. 2006. Physical coupling between lipids and proteins: a paradigm for cellular control. *Signal Transduct.* 6:112–132.
2. Dowhan, W. 1997. Molecular basis for membrane phospholipid diversity: why are there so many lipids? *Annu. Rev. Biochem.* 66:199–232.
3. Gruner, S. M. 1985. Intrinsic curvature hypothesis for biomembrane lipid composition: a role for nonbilayer lipids. *Proc. Natl. Acad. Sci. USA.* 82:3665–3669.
4. Cronan, J. E. 2003. Bacterial membrane lipids: where do we stand? *Annu. Rev. Microbiol.* 57:203–224.
5. Andersson, A. S., R. A. Demel, L. Rilfors, and G. Lindblom. 1998. Lipids in total extracts from *Acholeplasma laidlawii A* pack more closely than the individual lipids. Monolayers studied at the air-water interface. *Biochim. Biophys. Acta.* 1369:94–102.
6. Andersson, A. S., L. Rilfors, M. Bergqvist, S. Persson, and G. Lindblom. 1996. New aspects on membrane lipid regulation in *Acholeplasma laidlawii A* and phase equilibria of monoacyldiglucosyldiacylglycerol. *Biochemistry.* 35:11119–11130.
7. Morein, S., A. Andersson, L. Rilfors, and G. Lindblom. 1996. Wild-type *Escherichia coli* cells regulate the membrane lipid composition in a ''window'' between gel and non-lamellar structures. *J. Biol. Chem.* 271:6801–6809.
8. Goldfine, H. 1982. Lipids of prokaryotes; structure and distribution. *In* Current Topics in Membrane Transport, Vol. 17. S. Razin and S. Rottem, editors. Academic Press. New York. 1–43.
9. Ansell, G., J. N. Hawthorne, and R. M. C. Dawson. 1973. Form and Function of Phospholipids. Elsevier Science Publishers, Amsterdam.
10. McIntosh, T. J., and S. A. Simon. 2006. Roles of bilayer material properties in function and distribution of membrane proteins. *Annu. Rev. Biophys. Biomol. Struct.* 35:177–198.
11. Rilfors, L., and G. Lindblom. 2002. Regulation of lipid composition in biological membranes—biophysical studies of lipids and lipid synthesizing enzymes. *Colloids Surf. B Biointerfaces.* 26:112–124.
12. Attard, G. S., R. H. Templer, W. S. Smith, A. N. Hunt, and S. Jackowski. 2000. Modulation of CTP:phosphocholine cytidylyltransferase by membrane curvature elastic stress. *Proc. Natl. Acad. Sci. USA.* 97:9032–9036.
13. Krishnan, J., and P. A. Iglesias. 2004. A modeling framework describing the enzyme regulation of membrane lipids underlying gradient perception in *Dictyostelium* cells. *J. Theor. Biol.* 229:85–99.
14. Hamm, M., and M. M. Kozlov. 2000. Elastic energy of tilt and bending of fluid membranes. *Eur. Phys. J. E.* 3:323–335.
15. Zimmerberg, J., and M. M. Kozlov. 2006. How proteins produce cellular membrane curvature. *Nat. Rev. Mol. Cell Biol.* 7:9–19.
16. Helfrich, W. 1973. Elastic properties of lipid bilayers: theory and possible experiments. *Z Naturforsch.* 28(C):693–703.
17. May, S., and A. Ben-Shaul. 1999. Molecular theory of lipid-protein interaction and the L-α- H-II transition. *Biophys. J.* 76:751–767.
18. Osterberg, F., L. Rilfors, A. Wieslander, G. Lindblom, and S. M. Gruner. 1995. Lipid extracts from membranes of *Acholeplasma laidlawii A* grown with different fatty acids have a nearly constant spontaneous curvature. *Biochim. Biophys. Acta.* 1257:18–24.
19. Li, L., P. Storm, O. P. Karlsson, S. Berg, and A. Wieslander. 2003. Irreversible binding and activity control of the 1,2-diacylglycerol 3-glucosyltransferase from *Acholeplasma laidlawii* at an anionic lipid bilayer surface. *Biochemistry.* 42:9677–9686.
20. Lind, J., T. Ramo, M. L. Klement, E. Barany-Wallje, R. M. Epand, R. F. Epand, L. Maler, and A. Wieslander. 2007. High cationic charge and bilayer interface-binding helices in a regulatory lipid glycosyltransferase. *Biochemistry.* 46:5664–5677.
21. Razin, S., D. Yogev, and Y. Naot. 1998. Molecular biology and pathogenicity of mycoplasmas. *Microbiol. Mol. Biol. Rev.* 62:1094–1156.
22. Dowhan, W. 1997. CDP-diacylglycerol synthase of microorganisms. *Biochim. Biophys. Acta.* 1348:157–165.
23. Sparrow, C. P., and C. R. Raetz. 1985. Purification and properties of the membrane-bound CDP-diglyceride synthetase from *Escherichia coli*. *J. Biol. Chem.* 260:12084–12091.

24. Hirabayashi, T., T. J. Larson, and W. Dowhan. 1976. Membrane-associated phosphatidylglycerophosphate synthetase from *Escherichia coli*: purification by substrate affinity chromatography on cytidine 5′-diphospho-1,2-diacyl-*sn*-glycerol sepharose. *Biochemistry*. 15:5205–5211.
25. Carman, G. M., and D. S. Wieczorek. 1980. Phosphatidylglycerophosphate synthase and phosphatidylserine synthase activites in *Clostridium perfringens*. *J. Bacteriol.* 142:262–267.
26. Carman, G. M., R. L. Zaniewski, and J. J. Cousminer. 1982. CDP-diacylglycerol synthease activity in *Clostridium perfringens*. *Appl. Environ. Microbiol*. 43:81–85.
27. Berg, S., and A. Wieslander. 1997. Purification of a phosphatase which hydrolyzes phosphatidic acid, a key intermediate in glucolipid synthesis in *Acholeplasma laidlawii A* membranes. *Biochim. Biophys. Acta*. 1330:225–232.
28. Karlsson, O. P., A. Dahlqvist, S. Vikstrom, and A. Wieslander. 1997. Lipid dependence and basic kinetics of the purified 1,2-diacylglycerol 3-glucosyltransferase from membranes of *Acholeplasma laidlawii*. *J. Biol. Chem*. 272:929–936.
29. Vikstrom, S., L. Li, O. P. Karlsson, and A. Wieslander. 1999. Key role of the diglucosyldiacylglycerol synthase for the nonbilayer-bilayer lipid balance of *Acholeplasma laidlawii* membranes. *Biochemistry*. 38:5511–5520.
30. Edman, M., S. Berg, P. Storm, M. Wikstrom, S. Vikstrom, A. Ohman, and A. Wieslander. 2003. Structural features of glycosyltransferases synthesizing major bilayer and nonbilayer-prone membrane lipids in *Acholeplasma laidlawii* and *Streptococcus pneumoniae*. *J. Biol. Chem.* 278:8420–8428.
31. Brissette, J. L., E. A. Cabacungan, and R. A. Pieringer. 1986. Studies on the antibacterial activity of dodecylglycerol. Its limited metabolism and inhibition of glycerolipid and lipoteichoic acid biosynthesis in *Streptococcus mutans* BHT. *J. Biol. Chem.* 261:6338–6345.
32. Berg, S., M. Edman, L. Li, M. Wikstrom, and A. Wieslander. 2001. Sequence properties of the 1,2-diacylglycerol 3-glucosyltransferase from *Acholeplasma laidlawii* membranes. Recognition of a large group of lipid glycosyltransferases in eubacteria and archaea. *J. Biol. Chem.* 276:22056–22063.
33. Huijbregts, R. P., A. I. de Kroon, and B. de Kruijff. 1996. Rapid transmembrane movement of C6-NBD-labeled phospholipids across the inner membrane of *Escherichia coli*. *Biochim. Biophys. Acta.* 1280:41–50.
34. Almeida, P. F., W. L. Vaz, and T. E. Thompson. 2005. Lipid diffusion, free area, and molecular dynamics simulations. *Biophys. J.* 88:4434–4438.
35. Lindblom, G., G. Oradd, L. Rilfors, and S. Morein. 2002. Regulation of lipid composition in *Acholeplasma laidlawii* and *Escherichia coli* membranes: NMR studies of lipid lateral diffusion at different growth temperatures. *Biochemistry*. 41:11512–11515.
36. McElhaney, R. N., and M. E. Tourtellotte. 1970. Metabolic turnover of the polar lipids of Mycoplasma *laidlawii* strain B. *J. Bacteriol.* 101:72–76.
37. Keller, S. L., S. M. Bezrukov, S. M. Gruner, M. W. Tate, I. Vodyanoy, and V. A. Parsegian. 1993. Probability of alamethicin conductance states varies with nonlamellar tendency of bilayer phospholipids. *Biophys. J.* 65:23–27.
38. Fuller, N., and R. P. Rand. 2001. The influence of lysolipids on the spontaneous curvature and bending elasticity of phospholipid membranes. *Biophys. J.* 81:243–254.
39. Szule, J. A., N. L. Fuller, and R. P. Rand. 2002. The effects of acyl chain length and saturation of diacylglycerols and phosphatidylcholines on membrane monolayer curvature. *Biophys. J.* 83:977–984.
40. Leikin, S., M. M. Kozlov, N. L. Fuller, and R. P. Rand. 1996. Measured effects of diacylglycerol on structural and elastic properties of phospholipid membranes. *Biophys. J.* 71:2623–2632.
41. Fuller, N., C. R. Benatti, and R. P. Rand. 2003. Curvature and bending constants for phosphatidylserine-containing membranes. *Biophys. J.* 85:1667–1674.
42. Cornish-Bowden, A. 1995. Fundamentals of Enzyme Kinetics. Portland Press, London.
43. Carman, G. M., R. A. Deems, and E. A. Dennis. 1995. Lipid signaling enzymes and surface dilution kinetics. *J. Biol. Chem.* 270:18711–18714.
44. Romero, P. J., and L. de Meis. 1989. Role of water in the energy of hydrolysis of phosphoanhydride and phosphoester bonds. *J. Biol. Chem.* 264:7869–7873.
45. Wikstrom, M., J. Xie, M. Bogdanov, E. Mileykovskaya, P. Heacock, A. Wieslander, and W. Dowhan. 2004. Monoglucosyldiacylglycerol, a foreign lipid, can substitute for phosphatidylethanolamine in essential membrane-associated functions in *Escherichia coli*. *J. Biol. Chem.* 279:10484–10493.
46. Szeto, T. H., S. L. Rowland, L. I. Rothfield, and G. F. King. 2002. Membrane localization of MinD is mediated by a C-terminal motif that is conserved across eubacteria, archaea, and chloroplasts. *Proc. Natl. Acad. Sci. USA*. 99:15693–15698.
47. Szeto, T. H., S. L. Rowland, C. L. Habrukowich, and G. F. King. 2003. The MinD membrane targeting sequence is a transplantable lipid-binding helix. *J. Biol. Chem.* 278:40050–40056.
48. Mileykovskaya, E., I. Fishov, X. Fu, B. D. Corbin, W. Margolin, and W. Dowhan. 2003. Effects of phospholipid composition on MinD-membrane interactions in vitro and in vivo. *J. Biol. Chem.* 278:22193–22198.
49. Wieprecht, T., O. Apostolov, M. Beyermann, and J. Seelig. 1999. Thermodynamics of the α-helix-coil transition of amphipathic peptides in a membrane environment: implications for the peptide-membrane binding equilibrium. *J. Mol. Biol.* 294:785–794.
50. Christiansson, A., L. E. Eriksson, J. Westman, R. Demel, and A. Wieslander. 1985. Involvement of surface potential in regulation of polar membrane lipids in *Acholeplasma laidlawii*. *J. Biol. Chem.* 260: 3984–3990.
51. Mosior, M., and S. McLaughlin. 1992. Binding of basic peptides to acidic lipids in membranes: effects of inserting alanine(s) between the basic residues. *Biochemistry*. 31:1767–1773.
52. Lewis, R. N., and R. N. McElhaney. 2000. Surface charge markedly attenuates the nonlamellar phase-forming propensities of lipid bilayer membranes: calorimetric and (31)P-nuclear magnetic resonance studies of mixtures of cationic, anionic, and zwitterionic lipids. *Biophys. J.* 79:1455–1464.
53. Hristova, K., W. C. Wimley, V. K. Mishra, G. M. Anantharamiah, J. P. Segrest, and S. H. White. 1999. An amphipathic α-helix at a membrane interface: A structural study using a novel X-ray diffraction method. *J. Mol. Biol.* 290:99–117.
54. Wang, J., A. Gambhir, S. McLaughlin, and D. Murray. 2004. A computational model for the electrostatic sequestration of PI(4,5)P2 by membrane-adsorbed basic peptides. *Biophys. J.* 86:1969–1986.
55. Runarsson, T. P., and X. Yao. 2000. Stochastic ranking for constrained evolutionary optimization. *IEEE Trans. Evol. Comput.* 4:284–294.
56. Moles, C. G., P. Mendes, and J. R. Banga. 2003. Parameter estimation in biochemical pathways: A comparison of global optimization methods. *Genome Res.* 13:2467–2474.
57. Barkai, N., and S. Leibler. 1997. Robustness in simple biochemical networks. *Nature*. 387:913–917.
58. Cornell, R. B., and I. C. Northwood. 2000. Regulation of CTP:phosphocholine cytidylyltransferase by amphitropism and relocalization. *Trends Biochem. Sci.* 25:441–447.
59. Hauksson, J. B., L. Rilfors, G. Lindblom, and G. Arvidson. 1995. Structures of glucolipids from the membrane of *Acholeplasma laidlawii* strain A-EF22. III. Monoglucosyldiacylglycerol, diglucosyldiacylglycerol, and monoacyldiglucosyldiacylglycerol. *Biochim. Biophys. Acta*. 1258:1–9.
60. Andersson, A. S., L. Rilfors, G. Oradd, and G. Lindblom. 1998. Total lipids with short and long acyl chains from *Acholeplasma* form nonlamellar phases. *Biophys. J.* 75:2877–2887.
61. Jackowski, S. 1996. Cell cycle regulation of membrane phospholipid metabolism. *J. Biol. Chem.* 271:20219–20222.
62. Mileykovskaya, E., and W. Dowhan. 2005. Role of membrane lipids in bacterial division-site selection. *Curr. Opin. Microbiol.* 8:135–142.

63. Rothfield, L. I., Y. L. Shih, and G. King. 2001. Polar explorers: membrane proteins that determine division site placement. *Cell.* 106: 13–16.

64. Devaux, P. F. 1991. Static and dynamic lipid asymmetry in cell membranes. *Biochemistry.* 30:1163–1173.

65. Raetz, C. R., and E. P. Kennedy. 1973. Function of cytidine diphosphate-diglyceride and deoxycytidine diphosphate-diglyceride in the biogenesis of membrane lipids in *Escherichia coli*. *J. Biol. Chem.* 248: 1098–1105.

66. Alley, S. H., O. Ces, M. Barahona, and R. H. Templer. X-ray diffraction measurement of the monolayer spontaneous curvature of dioleoylphosphatidylglycerol. *Chem. Phys. Lipids.* In press.

67. Kooijman, E. E., V. Chupin, N. L. Fuller, M. M. Kozlov, B. de Kruijff, K. N. Burger, and P. R. Rand. 2005. Spontaneous curvature of phosphatidic acid and lysophosphatidic acid. *Biochemistry.* 44: 2097–2102.

68. Niemi, A. E., A. Andersson, L. Rilfors, G. Lindblom, and G. Arvidson. 1997. The effects of hydration and divalent cations on lamellar-nonlamellar phase transitions in membranes and total lipid extracts from *Acholeplasma laidlawii* A-EF22 - a ^{2}H NMR study. *Eur. Biophys. J.* 26:485–493.

69. Danino, D., A. Kaplun, G. Lindblom, L. Rilfors, G. Oradd, J. B. Hauksson, and Y. Talmon. 1997. Cryo-TEM and NMR studies of a micelle-forming phosphoglucolipid from membranes of *Acholeplasma laidlawii A* and *B*. *Chem. Phys. Lipids.* 85:75–89.

70. Wieslander, A., and L. Rilfors. 1977. Qualitative and quantitative variations of membrane lipid species in *Acholeplasma laidlawii A*. *Biochim. Biophys. Acta.* 466:336–346.

71. Archer, D. B., A. W. Rodwell, and E. S. Rodwell. 1978. The nature and location of *Acholeplasma laidlawii* membrane proteins investigated by two-dimensional gel electrophoresis. *Biochim. Biophys. Acta.* 513:268–283.

72. Vikstrom, S., L. Li, and A. Wieslander. 2000. The nonbilayer/bilayer lipid balance in membranes. Regulatory enzyme in *Acholeplasma laidlawii* is stimulated by metabolic phosphates, activator phospholipids, and double-stranded DNA. *J. Biol. Chem.* 275:9296–9302.

73. Mijakovic, I., S. Poncet, A. Galinier, V. Monedero, S. Fieulaine, J. Janin, S. Nessler, J. A. Marquez, K. Scheffzek, S. Hasenbein, W. Hengstenberg, and J. Deutscher. 2002. Pyrophosphate-producing protein dephosphorylation by HPr kinase/phosphorylase: a relic of early life? *Proc. Natl. Acad. Sci. USA.* 99:13442–13447.

74. Even, S., N. D. Lindley, and M. Cocaign-Bousquet. 2001. Molecular physiology of sugar catabolism in *Lactococcus lactis* IL1403. *J. Bacteriol.* 183:3817–3824.

75. Aiello, D. P., L. Fu, A. Miseta, and D. M. Bedwell. 2002. Intracellular glucose 1-phosphate and glucose 6-phosphate levels modulate Ca2+ homeostasis in *Saccharomyces cerevisiae*. *J. Biol. Chem.* 277:45751–45758.

76. Eisenberg, D. 1984. Three-dimensional structure of membrane and surface proteins. *Annu. Rev. Biochem.* 53:595–623.